This is an author's copy of an accepted manuscript to Sensors and Actuators A. Refer to the published copy (to be released) for the authoritative version.
Jaekwang Nam, Yung P. Lai, Lyle Gauthier, Gunhee Jang, and Eric Diller, "Resonance-based design of wireless magnetic capsule for effective sampling of microbiome in gastrointestinal tract," Sensors and Actuators A: Physical (accepted).

RESONANCE-BASED DESIGN OF WIRELESS MAGNETIC CAPSULE FOR EFFECTIVE SAMPLING OF MICROBIOME IN GASTROINTESTINAL TRACT

Jaekwang Nam [a, b], Yung P. Lai [b], Lyle Gauthier [b], Gunhee Jang [c] and Eric Diller [b, *]

[a] *School of Robotics, Kwangwoon University, Seoul 01890, South Korea.*

[b] *Department of Mechanical and Industrial Engineering, University of Toronto, Toronto, ON M5S 3G8, Canada.*

[c] *Department of Mechanical Engineering, Hanyang University, Seoul 04763, South Korea.*

Total Number of Pages: 24

Total Number of Tables: 1

Total Number of Figures: 15

Mailing Address:

Professor Eric Diller

Department of Mechanical and Industrial Engineering, University of Toronto, Toronto, ON M5S 3G8, Canada

E-mail: ediller@mie.utoronto.ca

ABSTRACT

This paper proposes a wireless magnetic capsule for effectively sampling the microbiome in the human gastrointestinal tract. Existing magnetically actuated sampling capsules suffer from limited actuation distance, which require a large magnetic field at least 14 mT for actuation. The capsule proposed in this work reduces the required magnetic field to 6 mT using a resonance-based design. This novel capsule contains two rotatable actuation magnets (AMs), whereby the attractive force between the two magnets increases in proportion to their angle, resulting in a magnetic spring whose stiffness can be tuned in the design process. To enable contamination-free preparation of the sampling space, sealing magnets are attached to covers to lock the capsule during GI-tract passage. The capsule opening mechanism is simulated using a physics-based model of the capsule actuation based on the magnetic spring design. According to the simulation results, a capsule with a size similar to that of existing ingestible capsules (length and height of 26 mm and 12.4 mm, respectively) is designed. The prototyped capsule comprises biocompatible materials, and its sampling and sealing ability are verified using a digestive material model. Results suggest that the capsule can enable effective sampling in the human gastrointestinal tract, with increased actuation distances.

KEYWORDS: Magnetic capsule, microbiome, sampling, wireless manipulation, resonance effect

1. INTRODUCTION

Trillions of microbiota including bacteria, archaea, fungi, protists, and viruses are found on and inside the human body, in areas such as the skin, lung, oral mucosa, and gastrointestinal (GI) tract [1,2]. This diverse population is known as the microbiome. Most of these diverse microorganisms reside in the GI tract, and the total weight of this population can be up to 2 kg [3]. The role of the microbiome in human health has been widely studied since the 1990s [4], and the gut microbiome has been characterized by a high diversity, elevated concentration, and many beneficial functions for the host health. These functions include regulating the immune system and protecting the gut from external pathogens by generating antimicrobial substances such as bateriocins [5,6]. Consequently, changes in the gut microbiome are associated with many diseases such as obesity [5–

7] and especially autoimmune diseases [8,9]. Thus, extensive investigation of the functions of the microbiome and its causality with diseases is being conducted. Because such research ideally requires the collection of multiple samples at various gut locations, effective sampling methods must be established considering the requirements of both the investigators and subjects.

As one of the simplest and convenient sampling method, endoscopes with mucosal biopsy capability have been investigated [10]. However, sampling through biopsy is uncomfortable and invasive and requires a trained operator. Moreover, several complications, such as wound infection and bleeding, may arise. In addition, it is challenging to insert the endoscope deep into the small intestine, as it is extremely far from both the anus and mouth. A more practical approach for collecting microbiome samples is to use a noninvasive wireless capsule. While simple capsules with onboard cameras have been used clinically since 2001 [11], there is no sampling capsule in clinical use. Capsules with integrated electronics have been explored because several tools such as electric actuators, light emitting diodes, and telemetry tracking systems can be exploited [12–14]. However, owing to the large battery and electronics volume, the space available for sample collection with such designs is limited. To solve this problem, an external magnetic field can be used to wirelessly charge the electric capsule [15,16] or directly drive the magnetic capsule [17–20]. Magnetic capsules are highly efficient because they directly use the external magnetic field to generate magnetic force or torque rather than converting the magnetic energy into electric energy. In such frameworks, the electrical system can be completely eliminated, and a compact capsule can be prepared. Considering these aspects, several researchers have developed magnetic sampling capsule. Finocchiaro et al. developed a magnetic capsule that is designed for the collection of microbiota's samples through mechanical brushing [18]. This capsule has a compact structure without any electronic components and is wirelessly activated by an external permanent magnet. However, it requires a strong magnetic field of 75 mT for operation. Shokrollahi et al. developed a blindly controlled magnetic capsule [20] which is driven by two onboard magnets, and contains a sampling space which is tightly sealed by the interaction force between the two magnets. Because this capsule does not use mechanical brushing mechanism, it requires a smaller magnetic field. However, it still requires a magnetic field of 15 mT to overcome the sealing force between the two magnets.

These required field strengths limit the utility of these methods, especially for larger patients. To reduce the required magnetic field for actuation, we developed a resonance-based magnetic sampling capsule, as shown in Fig. 1(a). Because the resonance effect maximizes the efficiency of the sampling mechanism, the capsule can be easily activated at the relatively low magnetic field of

6 mT. The proposed capsule has two rotatable magnets separated by a small gap, as shown in Fig. 1(c). This system functions as a magnetic spring because the magnets generate a restoring force through mutual attraction. This magnetic spring resonates at a frequency dependent on its stiffness, and the design relies on actuation at resonance for increased actuation amplitude with relatively low field strength. Although this capsule needs an additional power system to generate a time-varying magnetic field, the required intensity is half of that required by existing capsules [20]. Therefore, the capsule can be actuated at larger distances while using the same magnetic field generation system. Moreover, the proposed capsule can self-align and be blindly activated by an external magnetic field while the magnetic localization technology can be used for precise activation [21–25]. This paper presents the design along with a mathematical magnetic spring model to simulate the capsule in dynamic conditions. A prototype capsule was developed, and its activation, sampling, and sealing in a pseudo-digestive environment with a sludgy fluid similar to the human digestive fluid were experimentally evaluated.

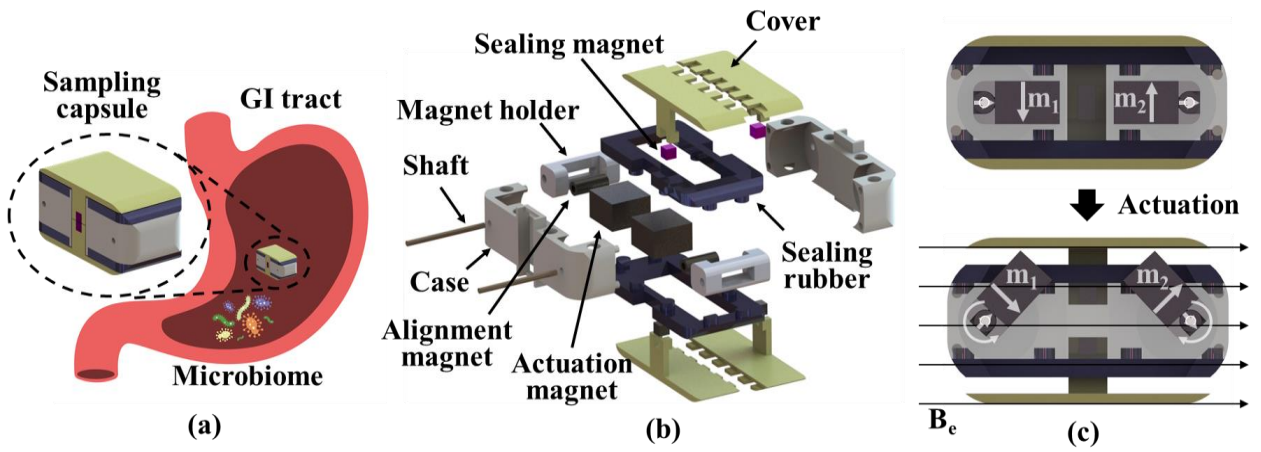

Figure 1. (a) Concept of the capsule for sampling the microbiome in the GI tract. (b) Components of the capsule. (c) Actuation of the capsule under an external magnetic field $\mathbf{B_e}$ ($\mathbf{m_1}$ and $\mathbf{m_2}$ are magnetic moments of the actuation magnets(AMs)).

2. CONCEPT OF THE CAPSULE

2.1 STRUCTURE OF THE CAPSULE

The proposed capsule is composed of pairs of components: two actuation magnets (AMs); two

alignment magnets; two magnet holders; two shafts; and two covers composed of two parts and four sealing magnets, as shown in Fig. 1(b). We design the body and cover in two parts and integrate them after assembling the inner components. Considering the vibration mechanism, a cubic body is chosen to minimize the volume of the capsule. The actuation and alignment magnets are attached to the magnet holder, which is integrated with the body using the shaft. The shaft is made of metallic titanium, and the other parts are made of plastic material or silicone rubber. Each cover has two sealing magnets, which tightly seal the capsule by attracting the sealing magnets placed on the opposite side. When an external magnetic field ($\mathbf{B}_e$) is applied to the capsule, the AMs are rotated by the magnetic torque and lift the covers up, as shown in Fig. 1(c). When an alternating magnetic field is applied, the AMs vibrate longitudinally and lift the upper and lower covers. During this lifting motion, the covers are guided to exhibit motion in a straight line by two slots on both sides of body.

2.2 ACTUATION PRINCIPLE

Figure 2 shows the magnetic torques and force applied to the left actuation magnet (AM1) by an external magnetic field and the magnetic field generated by the right actuation magnet (AM2) when a horizontal external magnetic field is applied along the x-axis. Each magnet has a magnetic moment vector ($\mathbf{m}_1$ or $\mathbf{m}_2$) and position vector ($\mathbf{r}_1$ or $\mathbf{r}_2$) that start from the rotating axis to the center point of the AMs. The two AMs are assumed to be symmetrically rotated. The total magnetic torque ($\mathbf{T}_1$) and their components applied on the AM1 can be expressed as

$$\mathbf{T}_1 = \mathbf{T}_{e1} + \mathbf{T}_{i1} + \mathbf{T}_{F1} \tag{1}$$

$$\mathbf{T}_{e1} = \mathbf{m}_1 \times \mathbf{B}_e \tag{2}$$

$$\mathbf{T}_{i1} = \mathbf{T}_{dipole}^{12}\left(\mathbf{r}_1, \mathbf{m}_1, \mathbf{r}_2, \mathbf{m}_2\right) \tag{3}$$

$$\mathbf{T}_{F1} = \mathbf{r}_1 \times \mathbf{F}_{i1} = \mathbf{r}_1 \times \mathbf{F}_{dipole}^{12}\left(\mathbf{r}_1, \mathbf{m}_1, \mathbf{r}_2, \mathbf{m}_2\right), \tag{4}$$

where $\mathbf{T}_{e1}$, $\mathbf{T}_{i1}$, $\mathbf{F}_{i1}$, and $\mathbf{T}_{F1}$ represent the magnetic torque generated by the external magnetic field, magnetic torque and force generated by the AM2, and torque generated by $\mathbf{F}_{i1}$, respectively. Each magnet is assumed to be a magnetic dipole. In this case, the magnetic torque and force generated by AM2 on AM1 can be expressed using the magnetic dipole model [26,27] as

$$\mathbf{T}_{\mathbf{dipole}}^{\mathbf{21}} = \frac{\mu_0}{4\pi\left\|\mathbf{r_{21}}\right\|^5}\left(3\mathbf{m_1}\times\left(\mathbf{m_2}\cdot\mathbf{r_{21}}\right)\mathbf{r_{21}} - \left\|\mathbf{r_{21}}\right\|^2\left(\mathbf{m_1}\times\mathbf{m_2}\right)\right) \tag{5}$$

$$\mathbf{F}_{\mathbf{dipole}}^{\mathbf{21}} = \frac{3\mu_0}{4\pi\left\|\mathbf{r_{21}}\right\|^4}\left(\left(\mathbf{r_{21}}\times\mathbf{m_2}\right)\times\mathbf{m_1} + \left(\mathbf{r_{21}}\times\mathbf{m_1}\right)\times\mathbf{m_2} - 2\mathbf{r_{21}}\left(\mathbf{m_2}\cdot\mathbf{m_1}\right) + 5\mathbf{r_{21}}\left(\left(\mathbf{r_{21}}\times\mathbf{m_2}\right)\cdot\left(\mathbf{r_{21}}\times\mathbf{m_1}\right)\right)\right), \tag{6}$$

where μ_0 and $\mathbf{r_{21}}$ represent the permeability of free space and the relative position vector of AM1 from AM2, respectively. The directions of torques indicated in Eqs. (2) and (3) are counterclockwise, because the each alignment torque for AM1 corresponds to the external magnetic field and the magnetic field from AM2, respectively. In contrast, the torque indicated in Eq. (4) has a clockwise direction because the N and S poles of the magnets attract each other. The torques generated by the two magnets, indicated in Eqs. (3) and (4), are the key idea of the capsule. The values of these torques change only with the angle of the magnet (θ) and do not depend on the external magnetic field. The summation of the two torques can be considered to correspond to a nonlinear magnetic spring, expressed as T_{spring} (θ). This torque of the magnetic spring can be rewritten using Hooke's law as

$$T_{i1} + T_{F1} = T_{spring}\left(\theta\right) = -k\left(\theta\right)\theta\,, \tag{7}$$

where k is the stiffness of the magnetic spring, which is a function of θ, and can thus be expressed as $k(\theta)$. In Fig. 2, all torque vectors of the capsule only have a z-directional component. Therefore, the torques indicated in Eq. (7) are z-directional torques. The stiffness k determines the resonant frequency of the capsule, and it can be adjusted through certain design variables, as discussed in Section 4.

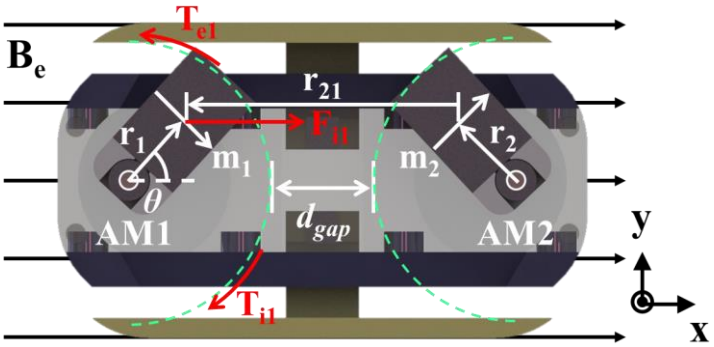

Figure 2. Magnetic torques and force applied on the left actuation magnet (AM1) by an external uniform magnetic field (B_e) and the right actuation magnet (AM2).

2.3 SELF-ALIGNMENT UNDER AN ARBITRARY EXTERNAL MAGNETIC FIELD

As shown in Figs. 1 (b) and (c), the capsule has two alignment magnets, the magnetic moments of which point to the positive *x*-direction. The net magnetic moment of the other two AMs is zero without an external magnetic field. Therefore, if an arbitrary external magnetic field is applied, owing to the magnetic moment of the alignment magnets, the body of the capsule aligns with the external magnetic field. Even if the AMs are vibrated and have non-zero net magnetic moment during operation, the capsule aligns along the external magnetic field because the two AMs only have *x*-directional net magnetic moment, as shown in Fig. 1(c).

2.4 SEALING ABILITY

It is necessary to prevent the contamination of the collected microbiome during sample transportation. Therefore, the capsule must be tightly sealed before and after sampling. To this end, sticky sealing rubber is inserted between the case and cover of the capsule. In addition, two sealing magnets are placed on each cover to generate an attractive magnetic force, as shown in Fig. 3. Notably, the sealing magnets do not significantly influence the AMs, because the net magnetic moment of the sealing magnets is zero. Moreover, the magnetic moment of the sealing magnets is nearly 36 times smaller than that of the AM, as indicated in Table I. Thus, the effect of the sealing magnets is not considered in Eq. (1). In addition, the possibility of the cover being opened and falling out of the capsule during sampling is considered. To prevent the loss of the covers, each cover has two hooks, as shown in Fig. 3. Because these hooks may obstruct the assembly, the covers are divided into two parts and integrated in the final process of the assembly.

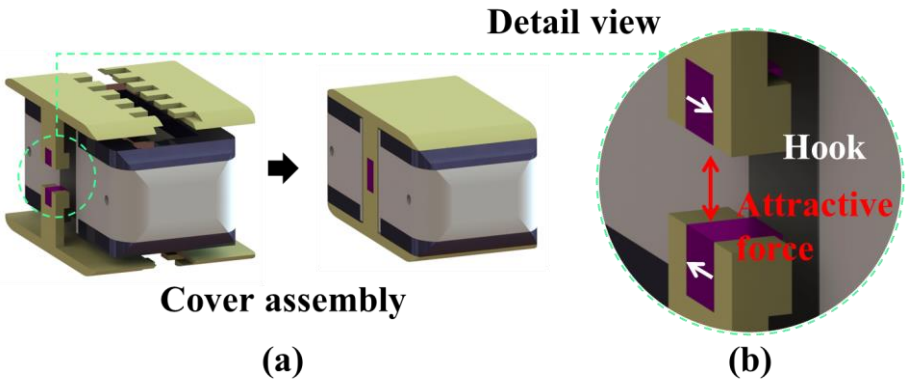

Figure 3. (a) Each cover is divided into two parts and integrated in the final process of assembly. (b) Sealing magnets are placed on each cover to generate attractive magnetic force, and hooks are used to prevent loss of the covers.

Table I. Properties of the magnets in the capsule.

Property	Volume (mm^3)	Grade	Magnetic moment ($A \cdot m^2$)
Actuation magnet	144.00 (L 6.00 × W 6.00 × H 4.00 mm)	N52 (B_r: 1.450 T)	166.16×10^{-3}
Sealing magnet	4.00 (L 1.59 × W 1.59 × H 1.59 mm)	N42 (B_r: 1.305 T)	4.64×10^{-3}
Alignment magnet	14.14 (D_o 2.00 × D_i 1.00 × H 6.00 mm)	N52 (B_r: 1.450 T)	16.31×10^{-3}

3. SELECTIVE ACTUATION UNDER DYNAMIC MAGNETIC FIELD

3.1 TORQUE OF THE MAGNETIC SPRING

The torque of the magnetic spring, indicated in Eq. (7), is analyzed to illustrate the basic concept of the capsule. The magnet specifications are summarized in Table I. The length of the position vectors ($\mathbf{r}_1$ and $\mathbf{r}_2$) is 4 mm, and the gap (d_{gap}) is 4 mm. The calculated torque components of the magnetic spring are shown in Fig. 4(a). T_{F1} is the main torque component of the magnetic spring because it generates a restoring torque against the rotational direction. T_{i1} disturbs the restoring

motion. When an external magnetic field is applied, AM1 rotates counterclockwise until it reaches a new equilibrium point, as shown in Fig. 4(b). When the external magnetic field is removed, the restoring torque acts on AM1, causing it to rotate clockwise. If an alternating magnetic field is applied, the AMs vibrate in both directions. This system is a type of mass spring system.

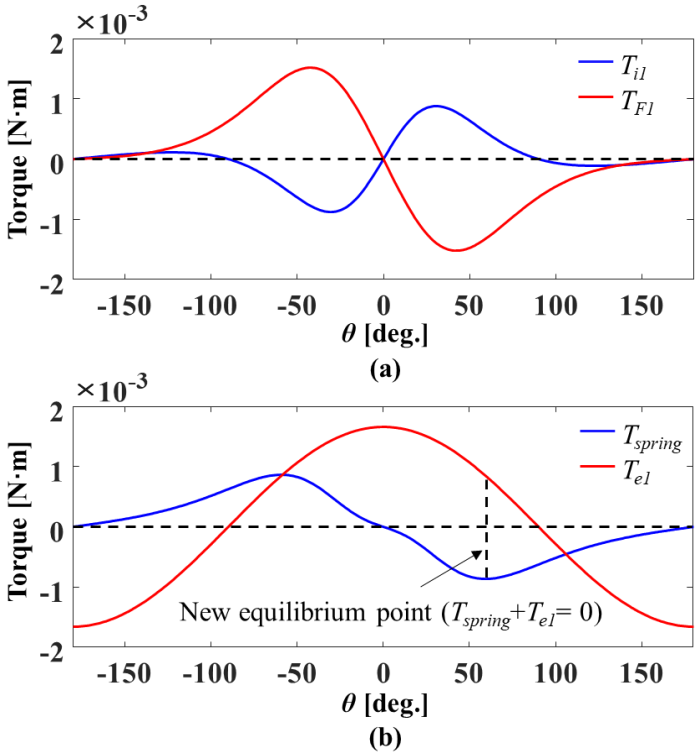

Figure 4. (a) Internal magnetic torque (T_{i1}) and torque (T_{F1}) generated by the internal magnetic force on AM1 vs θ. (b) Torque of magnetic spring (T_{spring}), which is the sum of T_{i1} and T_{F1}, and magnetic torque (T_{e1}) generated by an external magnetic field of 10 mT vs. θ.

3.2 EQUATION OF MOTION

To analyze the operation of the magnetic spring under an alternating magnetic field, the following nonlinear differential equation is defined as the equation of motion for AM1:

$$I\ddot{\theta} + 2\zeta\sqrt{k(\theta)I}\dot{\theta} + k(\theta)\theta = T_{e1} \tag{8}$$

$$\mathbf{T_{e1}} = \mathbf{m_1} \times \frac{B_e}{2}\left[\left(1+\sin\left(2\pi ft\right)\right) \quad 0 \quad 0\right]^T \tag{9}$$

where I, ζ, B_e, and f denote the rotational inertia of AM1, damping ratio, and amplitude and frequency of the alternating external magnetic field, respectively. In Eq. (9), the alternating field is considered to have a DC offset, and thus, it only exhibits a positive value in the x-direction. Because the capsule is aligned along the external magnetic field, the x-directional alternating field ensures that the capsule is aligned in the x-direction during the actuation.

3.3 APPROXIMATE STIFFNESS FUNCTION BASED ON THE FOURIER SERIES

The nonlinear differential equation presented as Eq. (8) is solved through a numerical analysis. We develop an approximate function instead of directly utilizing the complex stiffness function defined in Eq. (7). Considering T_{spring} to be a periodic function, the approximate stiffness function can be expressed using the Fourier series of T_{spring}:

$$k\left(\theta\right) = -T_{spring} / \theta = -\left(\sum_{k=1}^{n} A_k \cos\left(2\pi f_k \theta + \phi_k\right)\right) / \theta \tag{10}$$

where A_k, f_k, ϕ_k, and n are the amplitude, frequency, and phase of the kth cosine function and number of terms in the Fourier series, respectively. Each term in Eq. (10) can be quantified through the fast Fourier transform (FFT). For the transformation, T_{spring} in Eq. (7) is calculated for 3601 points in the bounded set $\theta \in [-2\pi, 2\pi]$. Next, several nonzero A_k are obtained, as shown in Fig. 5(a), which constitute the Fourier series presented in Eq. (10). Figure 5(b) shows the determined approximate stiffness function, which is in agreement with the exact stiffness function.

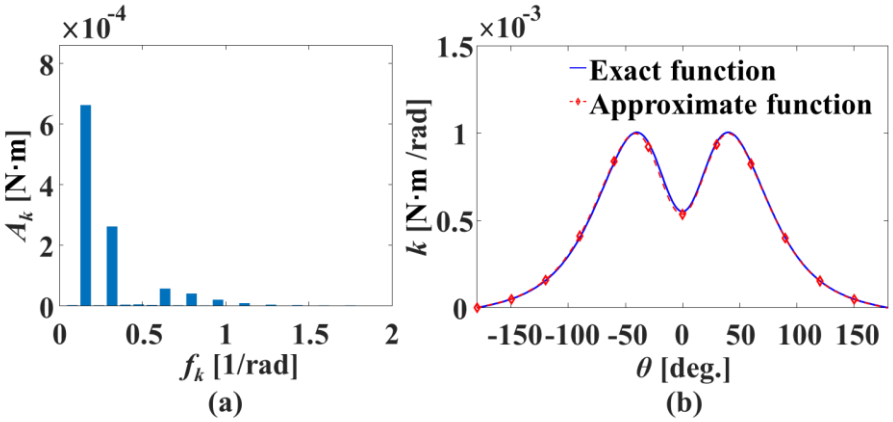

Figure 5. (a) A_k computed through the FFT analysis. (b) Comparison between the exact and approximate stiffness functions.

3.4 DYNAMIC SOLUTION

The stiffness function defined in Eq. (10) is used to numerically solve the equation of motion (Eq. (8)). The ode45 function of MATLAB, as a robust solver of differential equations, is used. The damping ratio (ζ) is set as 0.02, which is commonly used for rotational axes. Solutions corresponding to different B_e values are determined in the frequency domain, as shown in Fig. 6(a)

Figure 6(a) shows the effect of f on the absolute maximum angle or peak angle (θ_{peak}). The peak angle at the resonant point increases with the magnetic field intensity. However, the increase rate gradually decreases around 1 mT as the angle approaches 90°, because T_{e1} approaches zero near θ = 90°, as shown in Fig. 4(b). Furthermore, when the angle exceeds 90°, the external magnetic field generates a negative magnetic torque, which enhances the restoring motion. Therefore, if we increase the magnetic field intensity to more than 1 mT, the magnets do not function as a spring and tend to diverge. Notably, in the actual operating environment, the angle cannot exceed 90° over the magnetic field of 1 mT because the AMs may bump into the cover instead of diverging.

Because the magnetic spring has nonlinear stiffness, it exhibits several unique characteristics. First, the resonant points appear to be tilted to one side in Fig. 6(a), and their values depend on the amplitude of magnetic field. This phenomenon, which corresponds to the amplitude-dependent peak resonant frequency [28], must be considered to ensure that the magnetic spring operates under the accurate resonant frequency. Another characteristic known as the beating phenomenon can be observed in Fig. 6(b). Due to the spring's inconsistent stiffness as it vibrates, the wave exhibits an

interference pattern at each resonant frequency.

Figure 6(b) shows the solution of eq. (8) in the time domain at a resonant frequency of 18 Hz and B_e of 0.2 mT. The vibration is initially unstable in the transient state and gradually reaches the steady state. Because this effect is observed in the short transient state, we only consider the steady state data to calculate θ_{peak} in Fig. 6(a).

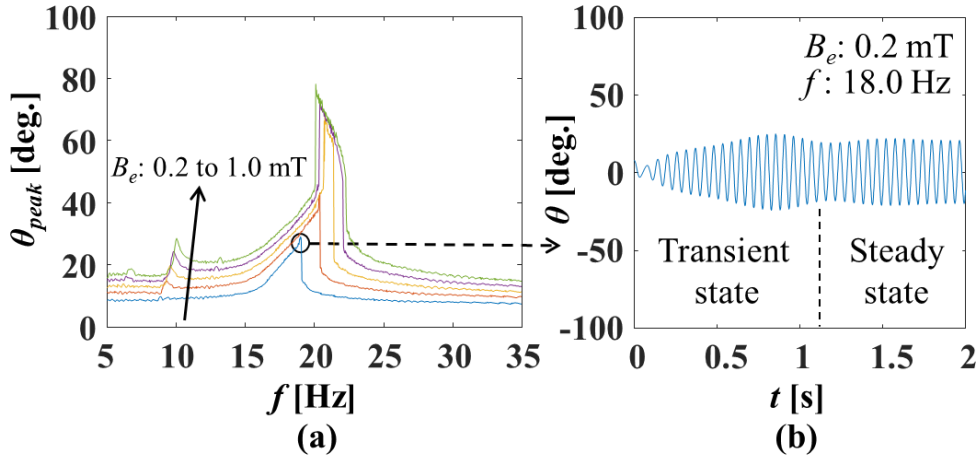

Figure 6. (a) Frequency and amplitude effect of the external magnetic field on θ_{peak}. (b) Solution of Eq. (8) at 18 Hz under an external magnetic field of 0.2 mT.

4. CAPSULE DESIGN

The effect of two design variables, d_{gap} and the length of $\mathbf{r_1}$, on the dynamic characteristics is analyzed, and the design strategy is established based on the results. Because the capsule has a symmetrical design, both the position vectors have the same length. Therefore, the length of $\mathbf{r_1}$ is used as a representative value. In the initial design, the length of $\mathbf{r_1}$ is 4 mm, and d_{gap} is 4 mm.

4.1 EFFECT OF d_{gap}

A key factor influencing the capsule is d_{gap} because the strength of the magnetic field is inversely proportional to the cube of the distance. Accordingly, the capsule's spring torque is inversely proportional to the gap within an angle of ±90°, as shown in Fig. 7(a). Because a higher spring

torque corresponds to a higher spring stiffness, as indicated in Eq. (7), the resonant frequency of the capsule is inversely proportional to the gap. Thus, the capsule with a smaller gap has a higher resonant frequency. However, the capsule with a smaller gap has a smaller amplitude, as shown in Fig. 7(b). The capsule with a larger gap can lift the cover more easily owing to the larger amplitude. However, if the gap is excessively large, the capsule size may increase. Furthermore, the AMs can be easily shaken by disturbances in the case of a large gap because the spring torque is required to resist undesired external forces. Therefore, it is necessary to select an adequate gap.

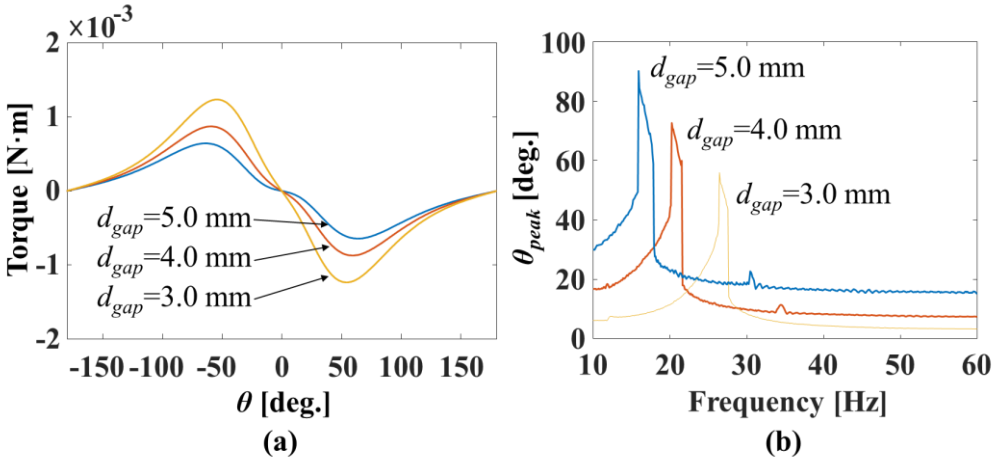

Figure 7. (a) Spring magnetic torque for various d_{gap}. (b) θ_{peak} under an external magnetic field of 0.8 mT with various d_{gap}.

4.2 EFFECT OF THE LENGTH OF $\mathbf{r_1}$

The effect of the length of $\mathbf{r_1}$ on the magnetic torque is shown in Fig. 8(a). A longer vector has a larger spring torque and thus a higher spring stiffness. Moreover, a longer $\mathbf{r_1}$ corresponds to a larger rotational inertia. These two effects are contrasting: The first and second effects increase and decrease the resonant frequency, respectively. However, the simulation result shows that the first effect is more notable, and the resonant frequency increases as the length of $\mathbf{r_1}$ increases, as shown in Fig. 8(b). Moreover, unlike d_{gap}, an increase in the length of $\mathbf{r_1}$ not only increases the magnitude of the torque, but also changes the torque waveform, as shown in Fig. 8(a). Consequently, the resonance is weak and indistinct, especially between 6.0 mm and 8.0 mm, as shown in Fig. 8(b). Thus, the smallest length (4.0 mm) can be an adequate value for $\mathbf{r_1}$.

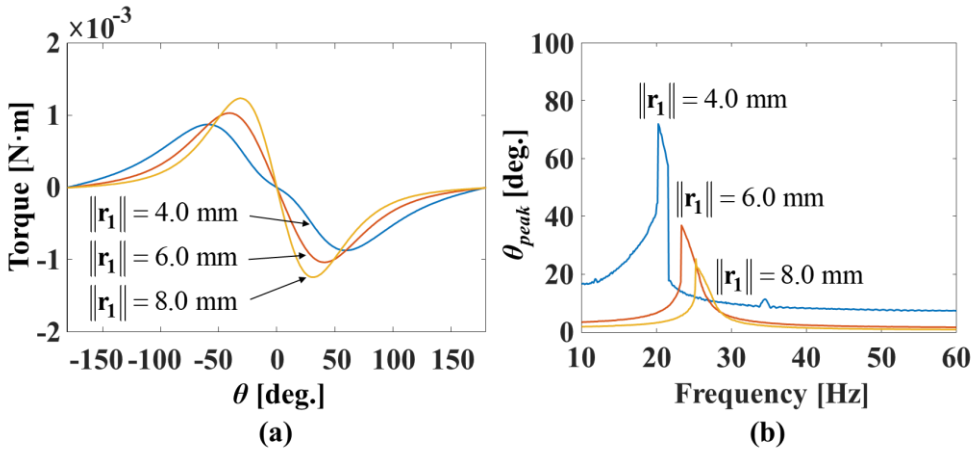

Figure 8. (a) Spring magnetic torque for various lengths of $\mathbf{r_1}$. (b) θ_{peak} under an external magnetic field of 0.8 mT with various length of $\mathbf{r_1}$.

4.3 CAPSULE DESIGN STRATEGY

The capsule design is informed by the analytical model results above. First, the median value of 4.0 mm is selected for d_{gap}. This value can produce a sufficiently large amplitude without prohibitively increasing the capsule size. The smallest length of 4.0 mm is selected for vector $\mathbf{r_1}$ because it corresponds to the maximum resonant amplitude and minimum capsule size. Figure 6 shows the simulation results obtained using these design variables. The capsule exhibits the largest amplitude at the resonant frequency of approximately 20 Hz. However, nonzero amplitudes are observed in the other frequency regions. In this case, if the height of the cover is not adequately large, the cover may be opened in the nonresonant region. In contrast, if the height is excessively large, the capsule cannot be activated even in the resonant region. Because this aspect is difficult to theoretically simulate, the adequate height of 10.3 mm was determined experimentally. With this height, the AMs can rotate 30° before contacting the cover, as shown in Fig. 9(a). In the experiment, the cover does not open until the alternating external magnetic field reaches 6 mT in the nonresonant region. At the resonance frequency, however, the cover starts to open from 2 mT. The maximum angle of the AMs is another design factor owing to its structural restriction, as shown Fig. 9(b). This angle should be as large as possible for the sampling, and it is set as 60°. The experiments demonstrate that this angle is adequate to extract a sample.

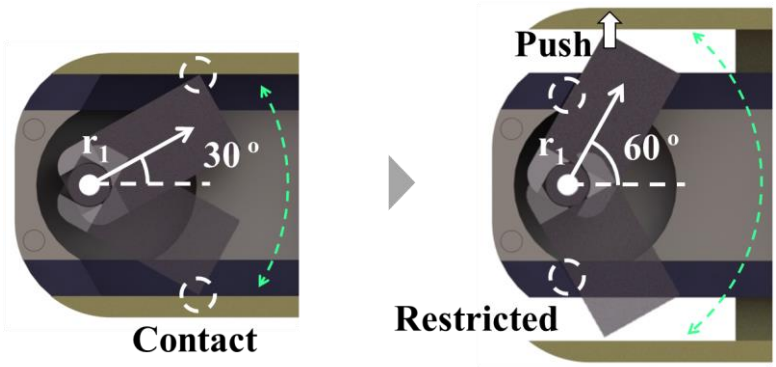

Figure 9. (a) The actuation magnets (AMs) start to contact with the cover as the angle reaches 30°. (b) The AMs rotate and push the cover until the maximum angle of 60°, restricted by the capsule structure.

5. EXPERIMENTS

5.1 FABRICATION AND EXPERIMENTAL SETUP

A prototype capsule was fabricated through 3D printing and silicone molding. The fabricated capsule was expected to be safe for human use and prevent the contamination of the collected samples during transportation. Thus, the biocompatibility of the material was considered. The printing parts were made of biocompatible plastic resin and fabricated using a 3D printer (Formlabs Form 3B). This resin was originally developed for long-term bodily contact and the safety was guaranteed by a U.S. Food and Drug Administration device master file. Although the silicone (Mold Star 16 FAST) was not developed for medical purposes, the biocompatibility of a similar silicone rubber (Mold Star 30) has been demonstrated by conducting several material tests including hydrophobicity analyses, acid resistivity tests, and cell viability tests [20].

Figure 10 shows the fabrication process of the proposed capsule. The sealing rubber to seal the capsule was manufactured using silicone molds, as shown in Figs. 10(a)–(d). The 3D printed mold consisted of two parts such that the liquid silicone could be molded between the concave and convex parts. The two parts of the liquid silicone were mixed and poured into the mold. After an hour, elastic silicone rubber was obtained. To minimize friction, titanium rods were used as the shafts. The other parts, including the covers, cases, and magnet holders, were 3D printed. The

printed cases and magnet holders were integrated with the shafts, AMs, and alignment magnets to form the middle part of the body, as shown in Fig. 10(e). Subsequently, the middle part of the body was integrated with silicone rubber. Because the two materials were challenging to bond, liquid silicone was poured over the entire capsule and cured. The prepared prototype capsule is shown in Fig. 10(h).

Figure 11 shows the experimental setup to evaluate the proposed capsule. Since this paper focuses on a novel capsule design, the conventional three-axis coil system which is commonly used for various magnetic robots was utilized [29], but a single-axis solenoid is enough to activate the capsule in practical situation because the capsule only needs one-dimensional magnetic field. The direction and amplitude of the external magnetic field were controlled using a joystick controller and control panel.

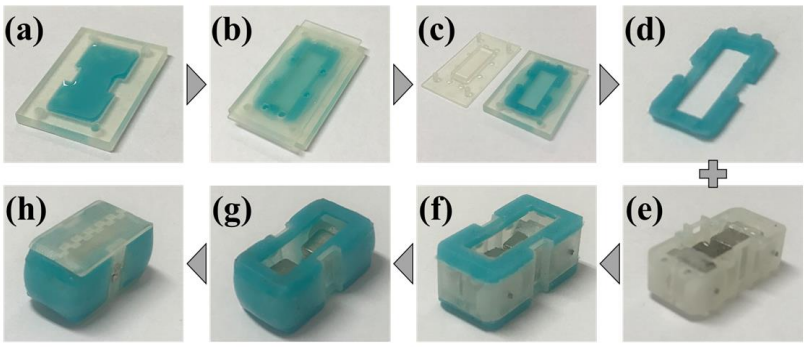

Figure 10. Fabrication of the proposed capsule. (a) Liquid silicone was poured into the lower mold. (b) The upper mold was covered with the lower mold to create concave and convex shapes of the silicone. (c) The liquid silicone was cured for an hour. (d) The cured silicone was demolded, and unnecessary residues were removed. (e) The middle part of the body was assembled using the cases, magnet holders, shafts, actuation magnets (AMs), and alignment magnets. (f) The cured sealing rubber was assembled with the middle part of the body. (g) Because the plastic material and silicone rubber were easily separated, liquid silicone was applied to the entire body. (h) Two covers with sealing magnets were assembled with the body.

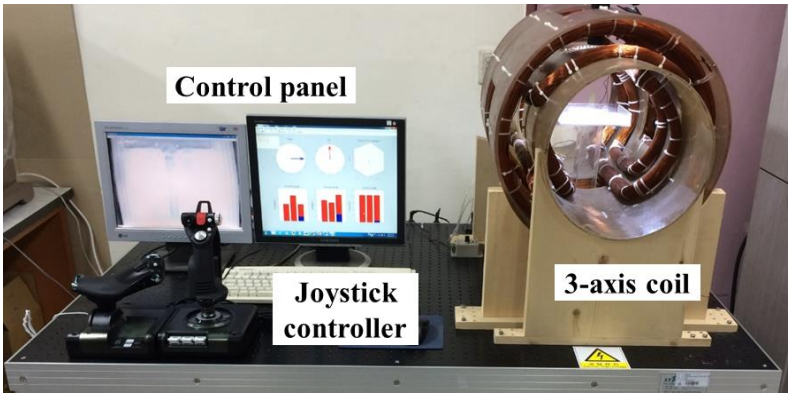

Figure 11. Experimental setup to generate and control an external magnetic field.

5.2 VIBRATION TEST

A free vibration test was performed to verify the resonant frequency of the proposed capsule. The capsule without a cover was bound to a rigid jig, and input force was applied to the AM. Subsequently, the free vibration of the AM was measured using a laser doppler vibrometer and fiber-optic interferometer, as shown in Fig. 12. The measured displacement was transferred to the signal analyzer. The transferred time domain signal was converted to the frequency domain, as shown in Fig. 13. The measured resonant frequency of 20.3 Hz was in agreement with the calculated frequency of 20.0 Hz.

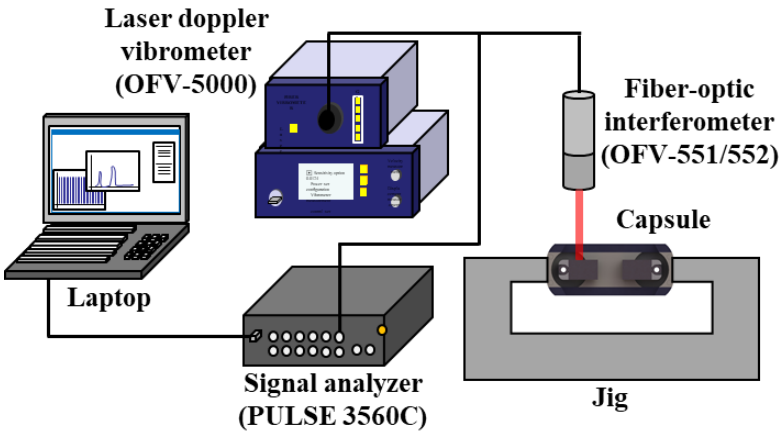

Figure 12. Experimental setup to measure the resonant frequency of the capsule using the free vibration.

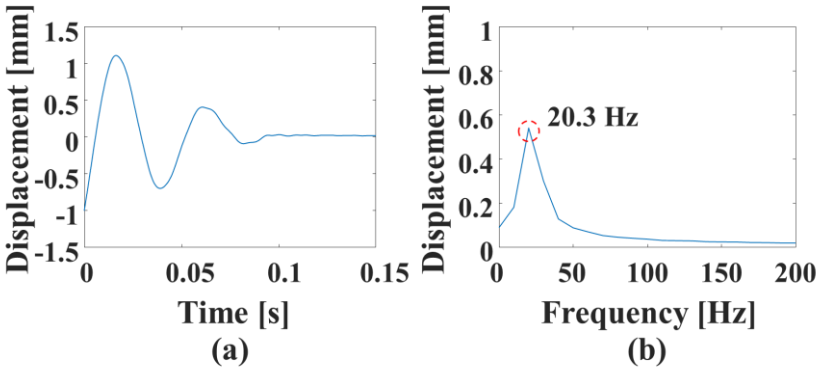

Figure 13. Measured displacement signal of the free vibrated capsule in the (a) time domain and (b) frequency domain.

5.3 SAMPLING TEST UNDER A DYNAMIC MAGNETIC FIELD

To efficiently generate a magnetic field without wasting energy, it is necessary to determine the minimum magnetic field required to activate the capsule. However, the theoretical determination of this magnetic field is challenging because complex factors such as the collision, friction, sealing force between the sealing magnets, and fluid viscosity must be considered. Thus, the required magnetic field was experimentally determined. To perform the test, a digesta was prepared by mixing ground feed and water in a 2:1 ratio, as shown in Fig. 14(a). This digesta could simulate the viscous environment in the gastrointestinal tract to ensure that the capsule was subjected to appropriate fluidic resistance. For ex vivo experiments, a 250 mm of porcine colon was filled with the digesta, and the capsule was placed into the colon. Then, dynamic magnetic fields were applied. The required magnetic field was measured by examining the point at which the digesta entered the capsule. The digesta began to enter the capsule from 4 mT. Moreover, the capsule could be aligned with the external magnetic field in that magnetic field, as shown in Fig. 14(b) and Supplementary Video. However, the minimum magnetic field of 4 mT was not sufficiently strong for the capsule to be aligned and extract an adequate amount of digesta sample in a brief period (approximately 10 seconds). We confirmed that 6 mT is a sufficiently strong magnetic field in the practical situation. In this magnetic field, the capsule was able to collect digesta sample about 80 % of the entire capacity (1500 mm^3) in 10 seconds. To reach 100 %, it took another 10 seconds. At magnetic field of less than 4 mT, the digesta could not enter the capsule because the sealing magnets tightly sealed

the capsule. To ensure the sealing ability, the capsule was exposed to an extreme vibration environment for 10 hours as shown in Fig. 15. The capsule was inserted in a tube filled with a digesta, and the tube was vibrated with an amplitude of 1.5 mm and a frequency of 10 Hz. After 10 hours, no digesta was observed in the capsule. Moreover, we observed the capsule performance at nonresonant frequencies. The capsule could perform sampling near the resonant frequency (± 1 Hz) when the magnetic field of 4 mT was applied. However, the capsule could not be activated in scenarios in which the difference from the resonant frequency was greater than 1 Hz.

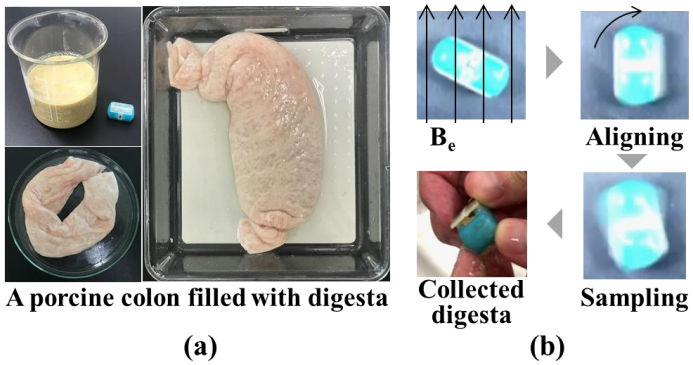

Figure 14. (a) Digesta sample prepared by mixing ground feed and water in a 2:1 ratio. A 250 mm of porcine colon was filled with digesta. The prototyped capsule was placed in the colon, and both ends of the colon were tied with wire. (b) Operation of the capsule. After the operation, the digesta was observed to be collected inside the body.

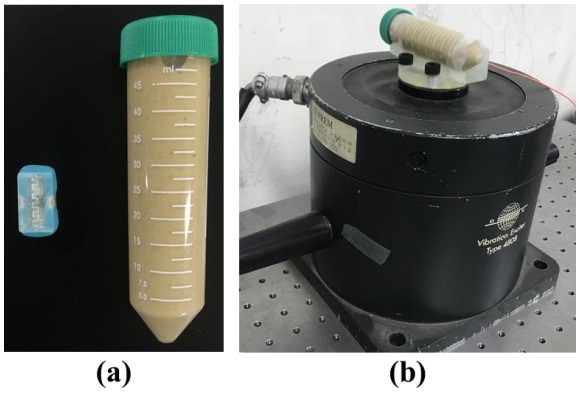

Figure 15. (a) Tube was filled with the digesta sample, and the capsule was inserted in the tube (b) The tube was vibrated for 10 hours while the vibration exciter vibrated with an amplitude of 1.5 mm and a frequency of 10 Hz. After 10 hours, no digesta was observed in the capsule.

6. CONCLUSION

The proposed wireless sampling capsule has a resonance-based design that can enable efficient sampling in the digestive system. Because the proposed capsule requires electromagnets and a power supply unit to generate an alternating magnetic field, the initial cost is higher than that of the other capsules operated by permanent magnets. However, this resonance-based design has notable potential applications. Although the resonance-based design is aimed only at decreasing the required external magnetic field, it can also be used to decrease the volume of AMs. In this case, the extra volume can be used to expand the sampling capacity or equip other medical functions such as biopsy and drug delivery. Moreover, the proposed capsule can be extended to exhibit multi-sampling capability by adding multiple resonant structures. This design can considerably decrease the time required for extracting multiple samples at various locations. Notably, the selective sampling at different resonant frequencies may be challenging because the magnets in the resonant structure will be magnetically coupled and interact with one another. It would be preferable to develop an improved capsule that can eliminate this issue or alternatively develop independent capsules with different resonant frequencies. Moreover, a capsule that can actively move in the digestive system can be developed to decrease the sampling time. In this context, the control of the proposed capsule is expected to be more efficient than that of the existing capsules, because the electromagnet system has a higher degree of freedom for control compared with the permanent magnet system. Consequently, future work can be aimed at developing an active capsule with multi-sampling capabilities.

FUNDING

This work was supported by the Connaught Fund at the University of Toronto; NSERC Discovery Grant under grant RGPIN-2020-04551; and Research Grant of Kwangwoon University in 2021.

REFERENCES

[1] J.R. Marchesi, J. Ravel, The vocabulary of microbiome research: a proposal, Microbiome 3 (2015) 1–3. https://doi.org/10.1186/s40168-015-0094-5.

[2] Y. Wang, B. Wang, J. Wu, X. Jiang, H. Tang, O.H. Nielsen, Modulation of gut microbiota in pathological states, Engineering 3 (2017) 83–89. https://doi.org/10.1016/J.ENG.2017.01.013.

[3] G. Lv, N. Cheng, H. Wang, The gut microbiota, tumorigenesis, and liver diseases, Engineering 3 (2017) 110–114. https://doi.org/10.1016/J.ENG.2017.01.017.

[4] J.M. Kinross, A.W. Darzi, J.K. Nicholson, Gut microbiome-host interactions in health and disease, Genome Med. 3 (2011) 14. https://doi.org/10.1186/gm228.

[5] R.E. Ley, P.J. Turnbaugh, S. Klein, J.I. Gordon, Human gut microbes associated with obesity, Nature 444 (2006) 1022–1023. https://doi.org/10.1038/4441022a.

[6] P.J. Turnbaugh, R.E. Ley, M.A. Mahowald, V. Magrini, E.R. Mardis, J.I. Gordon, An obesity-associated gut microbiome with increased capacity for energy harvest, Nature 444 (2006) 1027–1031. https://doi.org/10.1038/nature05414.

[7] R.E. Ley, F. Bäckhed, P. Turnbaugh, C.A. Lozupone, R.D. Knight, J.I. Gordon, Obesity alters gut microbial ecology, Proc. Natl. Acad. Sci. USA. 102 (2005) 11070–11075. https://doi.org/10.1073/pnas.0504978102.

[8] J.S. Biteen, P.C. Blainey, Z.G. Cardon, M. Chun, G.M. Church, P.C. Dorrestein, S.E. Fraser, J.A. Gilbert, J.K. Jansson, R. Knight, J.F. Miller, A. Ozcan, K.A. Prather, S.R. Quake, E.G. Ruby, P.A. Silver, S. Taha, G. van den Engh, P.S. Weiss, G.C.L. Wong, A.T. Wright, T.D. Young, Tools for the microbiome: nano and beyond, ACS Nano. 10 (2016) 6–37. https://doi.org/10.1021/acsnano.5b07826.

[9] M.H. McLean, D. Dieguez, L.M. Miller, H.A. Young, Does the microbiota play a role in the pathogenesis of autoimmune diseases? Gut. 64 (2015) 332–341. https://doi.org/10.1136/gutjnl-2014-308514.

[10] S.A. Fillon, J.K. Harris, B.D. Wagner, C.J. Kelly, M.J. Stevens, W. Moore, R. Fang, S.

Schroeder, J.C. Masterson, C.E. Robertson, N.R. Pace, S.J. Ackerman, G.T. Furuta, Novel device to sample the esophageal microbiome—the esophageal string test, PLoS One. 7 (2012) e42938. https://doi.org/10.1371/journal.pone.0042938.

[11] M. Halpern, H. Jacob, Atlas of capsule endoscopy. Yoqneam, Israel: Given Imaging, Inc, Ltd. (2002).

[12] G. Ciuti, A. Menciassi, P. Dario, Capsule endoscopy: from current achievements to open challenges, IEEE Rev. Biomed. Eng. 4 (2011) 59–72. https://doi.org/10.1109/RBME.2011.2171182.

[13] A. Koulaouzidis, D.K. Iakovidis, A. Karargyris, E. Rondonotti, Wireless endoscopy in 2020: Will it still be a capsule?, World J Gastroenterol. 21 (2015) 5119–5130. https://doi.org/10.3748/wjg.v21.i17.5119.

[14] J. Cui, X. Zheng, W. Hou, Y. Zhuang, X. Pi, J. Yang, The study of a remote-controlled gastrointestinal drug delivery and sampling system, Telemed. J E Health. 14 (2008) 715–719. https://doi.org/10.1089/tmj.2007.0118.

[15] M.R. Basar, M.Y. Ahmad, J. Cho, F. Ibrahim, An improved resonant wireless power transfer system with optimum coil configuration for capsule endoscopy, Sens. Actuator A Phys. 249 (2016) 207–216. https://doi.org/10.1016/j.sna.2016.08.035.

[16] J. Gao, G. Yan, Z. Wang, P. Jiang, D. Liu, A capsule robot powered by wireless power transmission: Design of its receiving coil, Sens. Actuator A Phys. 234 (2015) 133–142. https://doi.org/10.1016/j.sna.2015.08.021.

[17] M. Simi, G. Gerboni, A. Menciassi, P. Valdastri, Magnetic Torsion Spring Mechanism for a Wireless Biopsy Capsule, Journal of Medical Devices. 7 (2013). https://doi.org/10.1115/1.4025185.

[18] M. Finocchiaro, C. Giosuè, G. Drago, F. Cibella, A. Menciassi, M. Sprovieri, G. Ciuti, Design of a magnetic actuation system for a microbiota-collection ingestible capsule, in: 2021 IEEE International Conference on Robotics and Automation (ICRA), 2021: pp. 6905–6911. https://doi.org/10.1109/ICRA48506.2021.9561142.

[19] S. Yim, E. Gultepe, D.H. Gracias, M. Sitti, Biopsy using a Magnetic Capsule Endoscope Carrying, Releasing, and Retrieving Untethered Microgrippers, IEEE Transactions on Biomedical Engineering. 61 (2014) 513–521.

https://doi.org/10.1109/TBME.2013.2283369.

[20] P. Shokrollahi, Y.P. Lai, S. Rash-Ahmadi, V. Stewart, M. Mohammadigheisar, L.-A. Huber, N. Matsuura, A.E.H. Zavodni, J. Parkinson, E. Diller, Blindly controlled magnetically actuated capsule for noninvasive sampling of the gastrointestinal microbiome, IEEE/ASME Trans. Mechatron. (2020) 1–1. https://doi.org/10.1109/TMECH.2020.3043454.

[21] W. Andrä, H. Danan, W. Kirmsse, H.H. Kramer, P. Saupe, R. Schmieg, M.E. Bellemann, A novel method for real-time magnetic marker monitoring in the gastrointestinal tract., Phys Med. Biol. 45 (2000) 3081–3093. https://doi.org/10.1088/0031-9155/45/10/322.

[22] C. Hu, M.Q.-H. Meng, M. Mandal, Efficient magnetic localization and orientation technique for capsule endoscopy, Int. J. Inf. Acquis. 02 (2005) 23–36. https://doi.org/10.1142/S0219878905000398.

[23] S. Yim, M. Sitti, 3-D localization method for a magnetically actuated soft capsule endoscope and its applications, IEEE Trans. Robot. 29 (2013) 1139–1151. https://doi.org/10.1109/TRO.2013.2266754.

[24] D. Son, S. Yim, M. Sitti, A 5-D localization method for a magnetically manipulated untethered robot using a 2-D array of hall-effect sensors, IEEE/ASME Trans. Mechatron. 21 (2016) 708–716. https://doi.org/10.1109/TMECH.2015.2488361.

[25] X. Wu, W. Hou, C. Peng, X. Zheng, X. Fang, J. He, Wearable magnetic locating and tracking system for MEMS medical capsule, Sens. Actuator A Phys. 141 (2008) 432–439. https://doi.org/10.1016/j.sna.2007.10.051.

[26] P.B. Landecker, D.D. Villani, K.W. Yung, An analytic solution for the torque between two magnetic dipoles, Phys. Sep. Sci. Eng. (1999). https://doi.org/10.1155/1999/97902.

[27] D.D. Villani, An analytic solution for the force between two magnetic dipoles, Magn. Electr. Sep. 9 (1998) 39–52.

[28] L.D. Landau, E.M. Lifshitz, Mechanics, Elsevier Science, 1982.

[29] S. Jeon, G. Jang, H. Choi, S. Park, Magnetic navigation system with gradient and uniform saddle coils for the wireless manipulation of micro-robots in human blood vessels, IEEE Trans. Magn. 46 (2010) 1943–1946.

https://doi.org/10.1109/TMAG.2010.2040144.